Materials Today Communications 32 (2022) 104127

Contents lists available at ScienceDirect

Materials Today Communications

journal homepage: www.elsevier.com/locate/mtcomm

Phononic crystal based sensor to detect acoustic variations in methyl & ethyl nonafluorobutyl ether

Muhammad [a,b,*,1]

[a] Department of Mechanical, Manufacturing and Biomedical Engineering, Trinity College Dublin, College Green, Dublin 02 D02 PN40, Ireland
[b] Department of Architecture and Civil Engineering, City University of Hong Kong, Tat Chee Avenue, Kowloon, Hong Kong Special Administrative Region

ARTICLE INFO

Keywords:
Fano resonance
Wave interference
Phononic crystal
Metamaterials
Sensors

ABSTRACT

Phononic crystals and metamaterials have been widely studied for wave manipulation applications. In this study, we propose a conceptual framework for a new type of acoustic bio-chemical sensor that works based on the principle of phononic crystals and metamaterials to detect the temperature and pressure changes in active solvents like Methyl Nonafluorobutyl Ether (MNE) and Ethyl Nonafluorobutyl Ether (ENE). First, a wide low-frequency bandgap is obtained from the proposed composite unit cell structure with trampoline effect. Then a defect is introduced to adjust the localize cavity modes inside the reported bandgap. Later, the cavity is filled with MNE and ENE solvents that eventually resulted into fluid-solid coupling physics. The numerical wave dispersion curves and transmission profiles show presence of Fano-like interference/resonance effect evident from the observation of asymmetrical transmission profile. Such robust asymmetrical transmission peak is generated due to coupling of incident waves with scattered wave field emitted from the MNE and ENE solvents upon excitation. The variation in acoustic properties of MNE and ENE caused by temperature and pressure fields on newly born Fano-like asymmetrical transmission profile is studied. The proposed acoustic bio-chemical sensor governed by Fano-interference effect efficiently capture the variation in acoustic properties of MNE and ENE solvents at relatively low-frequency regime that makes this approach favorable for sensing applications. Such smart acoustic bio-chemical sensors can have useful applications in pharmaceutical production, petrochemicals and capturing ingredients of cosmetic and beauty products.

1. Introduction

Wave manipulation by artificial composite materials so-called phononic crystals (PnCs) and metamaterials have observed a surge of research studies in acoustics, mechanics, solid-state physics, condensed matter physics and material science due to peculiar wave dispersion and dynamic properties that are inconceivable from naturally occurring materials. Particularly, they exhibit frequency bandgap (BG) where wave propagation is obstructed either due to Bragg effect [1] or local resonance mechanism [2]. The fundamental properties and applications of PnCs and metamaterials have been discussed in number of review articles ranging from sound insulation to earthquake applications and telecommunication devices based on localized modes inside the waveguide [3,4]. Apart from the BG property, PnC sensor is an emerging research topic with prominent applications in multiple fields like pharmaceutical production, petrochemicals, water and air pollution detection etc. These sensors are able to detect the changes in acoustic properties stimulated by environmental factors like temperature, humidity, pressure etc.

Thanks to BG attribute of PnCs that facilitates defect formation resulting into wave energy localization. For instance, Arafa Hussein Aly et al. [5] studied 1-D PnC with defect state. The sensitivity and wave energy localization of defect mode (transmission peak) is tuned by adjusting the piezoelectric and piezomagnetic defect layers. In another work, Nagaty et al. [6] studied the effect of temperature on properties of 1-D piezoelectric PnC. The study deduced that temperature play an important role in tuning the BG and, positing the local resonant frequencies, depending upon the presence of piezoelectric material. Likewise, in another work Arafa Hussein Aly et al. [7] studied the significance of temperature on performance of piezoelectric energy

* Corresponding author at: Department of Mechanical, Manufacturing and Biomedical Engineering, Trinity College Dublin, College Green, Dublin 02 D02 PN40, Ireland.
E-mail addresses: Dr.Muhammad@tcd.ie, fmuhammad6-c@my.cityu.edu.hk.
[1] ORCID ID: 0000-0003-3492-0123

https://doi.org/10.1016/j.mtcomm.2022.104127
Received 16 May 2022; Received in revised form 22 July 2022; Accepted 27 July 2022
Available online 29 July 2022

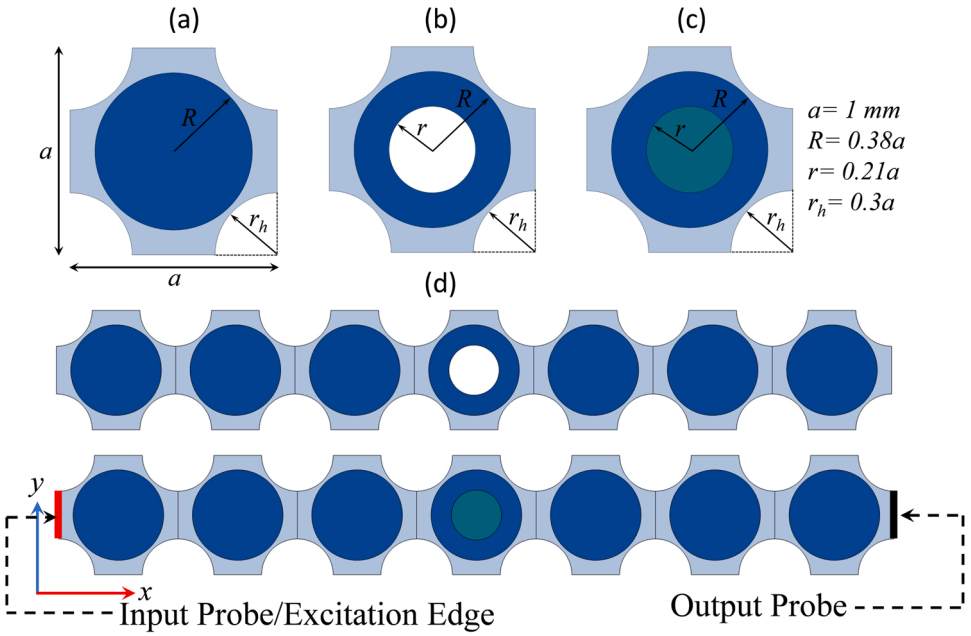

Fig. 1. Unit cell structure of PnC (a) basic unit cell design (b) with cavity (c) the air cavity is filled with some liquid like MNE/ENE (d) array of unit cell structures for supercell modal analysis and frequency response studies. In the bottom row, the cavity is filled with active solvent like MNE or ENE. All the geometric parameters are given at the inset of figure.

harvester PnC. The reported results showed strong effect of temperature on performance of energy harvester.

Recently, some researchers have reported lab-on-chip biosensor for manipulating Lamb wave in thin plate [8] and surface acoustic wave (SAW) in semi-infinite half-space [9]. PnC based smart sensor is recently reported by Gharibi et al. [10] to sense the acoustic properties in different water-ethanol mixtures. In another work, Gharibi and Mehaney [11] proposed a 2-D PnC sensor for volumetric detection of hydrogen peroxide in liquids. PnC sensor can also be applied for detecting the concentration of Sodium Iodide (NaI) in water [12]. The proposed sensor is comprised of stainless-steel matrix with periodic array of holes filled with water. The resonance frequencies confined to the NaI waveguide embedded in the center of sensor device serves as sensing mechanism. The localized defect mode is set inside the BG that allows robust wave propagation inside the BG frequency region. Likewise multiple other 2-D and 3-D PnC biosensors have been studied both theoretically and experimentally. Another example include the work by Oseev et al. [13] where PnC sensor is developed to detect the physical properties of gasoline and determine the octane numbers. For solid-liquid interaction, Jin et al. [14] proposed hollow-pillar filled with some liquid resting on thin elastic plate and investigated the whispering gallery modes for temperature sensing application. Similarly, Mukhin et al. [15] developed PnC based liquid sensor by proposing the concept of narrow band solid-liquid composite arrangement.

Fano interference/resonance (asymmetrical transmission peaks caused by wave scattering) was theoretically discussed by Ugo Fano in one of the quantum mechanical study on autoionizing resonance in atoms [16]. It is a resonance that is quite different from other "true" resonance like Fabry–Perot resonances or Mie resonances. Therefore, it is unclear who first use this term "Fano resonance" and as recently explained by Mikhail F. Limonov [17], a better term can be "Fano interference". Because Fano effect is nothing more than an interference caused by interaction of incident and scattered wave fields. The interference of two oscillators with different damping rates results into broad and narrow spectral shapes that made it most amazing "resonance" effect in physics [17,18]. Moreover, the phenomenon of interference does not require prerequisite conditions that occur in "true" resonance including the presence of resonator. Therefore, in this work we will use the term "Fano interference" as an alternate to Fano resonance that is extensively used in the literature. Since pioneering work by Ugo Fano [16], it is widely studied in both quantum and classical systems and exhibition of Fano interference is observed in photonic crystals, optics, plasmonic nanostructures and metamaterials [19,20]. As a universal mechanism, it is witnessed in many areas of wave particle physics. More recently, Fano interference is also reported in phononic structures [21–24]. Further details about complex dynamic properties revealed by Fano interference effect and applications can be found in [17,19,25]. Briefly, some prominent applications include refractive index sensing particularly in biological applications [26], temperature, pressure and displacement sensors [19], active switching [27], beam filtering, Rayleigh and Lamb waves manipulation [22,28] etc. Fano interference's sharp spectral characteristics and robust field enhancements are frequently used in these applications.

Recently, Fano interference phenomena are explored in PnCs and acoustic metamaterials like locally resonant structures [29], multilayer ridge structures [23,28,30], periodic hollow cylindrical array [31], pillared structure [22] etc. Jin et al. [22] varied the geometric parameters for a pair of pillars to study Fano interference upon Lamb wave interaction. Most of these works have discussed complex dynamic properties of Fano interference in PnCs. The scattered wave fields emitted by the PnC provides useful information about Fano-like interference effect. The emitted wave field is subtraction of incident wave energy before interaction with PnCs and transmitted wave energy after interaction. The destructive interference between the emitted and incident waves, when the emitted wave's amplitude is comparable to the incident wave, causes Fano asymmetric transmission.

In this paper, we are specifically interested in a new application of Fano interference asymmetrical profile in PnCs as an acoustic biochemical sensor to sense the acoustic variations in active solvents like Methyl Nonafluorobutyl Ether (MNE) and Ethyl Nonafluorobutyl Ether (ENE). However, the study findings is not limited to these two types of active solvents, perhaps it can be applied to other bio-chemicals too, provided that acoustic properties are known. The introduction of solvents in the PnC unit cell structure resulted into localize modes. A keen observation of wave transmission spectrum revealed presence of low-frequency asymmetric sharp transmission profile that is associated to

Table 1
Material parameters.

	Young Modulus (GPa)	Mass density (kg/m^3)	Poisson ratio
Epoxy	3.5	1250	0.35
Tungsten	411	19,350	0.28

Fano resonance resulting from interference phenomena between incident wave and scattered wave fields emitted by MNE and ENE solvents. Such asymmetric transmission profile is very robust with minimal losses that makes the PnC most suitable for sensing applications. MNE is an organic solvent that is extensively used in beauty products [32]. The low surface tension, high boiling point make it a potential candidate for cleaning solvents and lubricants. Furthermore, it is non-flammable, non-toxic, colorless, and clear liquid that makes it also suitable for industrial and pharmaceutical applications [33]. ENE is also refereed as eco-friendly solvent with prominent applications in chromatography due to its high lipophilic character. It is also used as a biochemical in proteomics research.

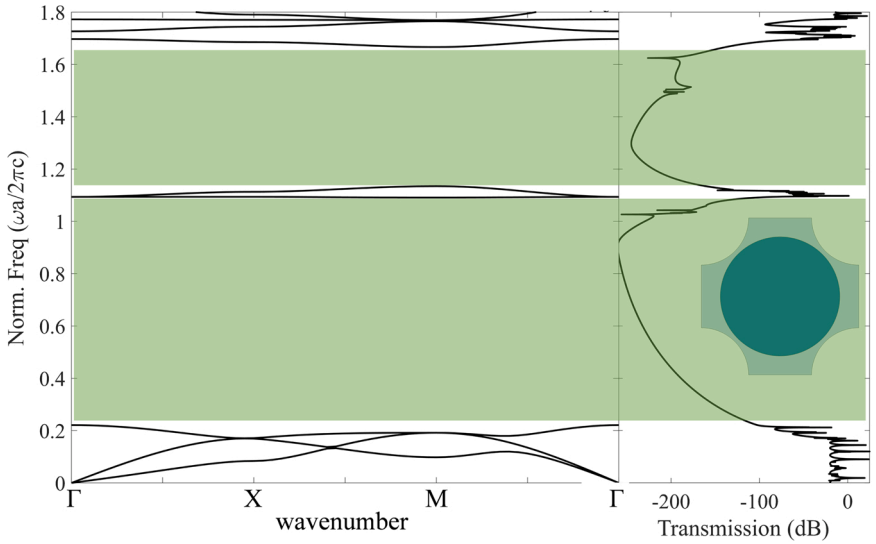

Fig. 2. Dispersion plot and wave transmission curve of PnC parent unit cell structure with BGs highlighted.

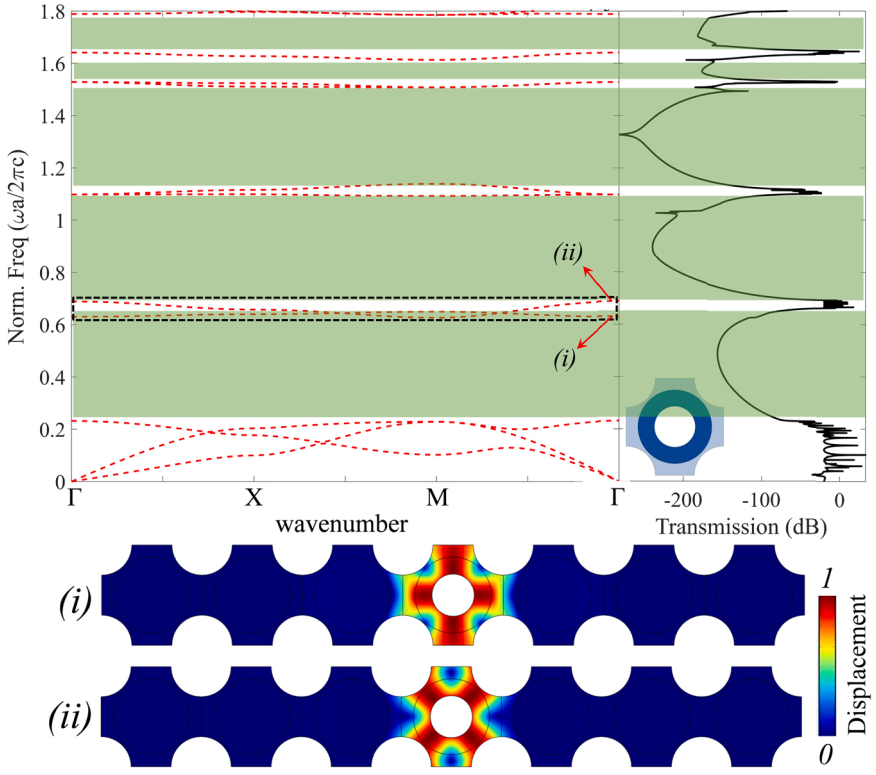

Fig. 3. Wave dispersion curve and transmission spectrum with BGs for hollow PnC unit cell structure. The introduction of hole inside the Tungsten inclusion gives birth to two new passbands at the center of first BG. The displacement field plots show that they are localize mode of the hollow inclusion. Since these bands are present in the BG frequency region, wave energy localization is observed inside the cavity and no wave propagation is observed in the neighboring parent unit cell structures.

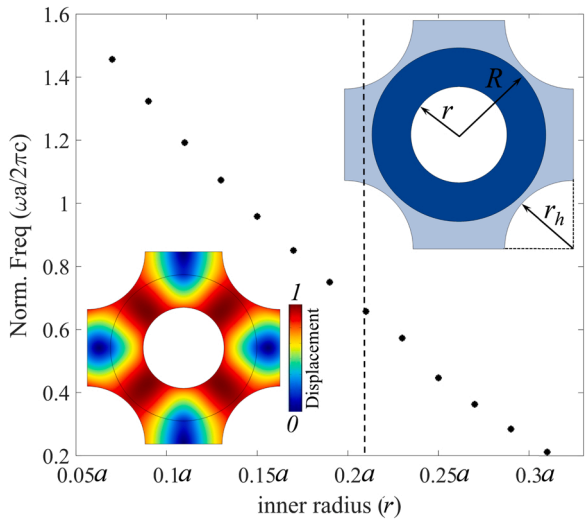

Fig. 4. Effect of hole radius *r* on the localize bands available inside the first BG.

Despite the fascinating findings, potential application of PnCs in biochemical sensing applications is still maturing. Almost none of the studies have applied Fano interference effect for cosmetic applications where most of the chemicals are liquids and acoustic properties is dependent on the density and wave velocity that varies with change in temperature, pressure and other environmental factors. Here in this study, we employed the concept of Fano interference to sense the variation in acoustic properties of MNE and ENE solvents. We first proposed a unit cell structure design that consist of epoxy matrix with tungsten inclusion and achieve low-frequency wide BG. Later, a cavity is introduced to localize the newly born passbands inside the reported BG region. These are localized quadrupolar modes induced by introduction of holes. In literature such modes are also referred as whispering gallery modes [35,36]. Then, MNE and ENE solvents are filled inside the cavity of proposed PnCs for sensing applications. The change in temperature and pressure field affect the acoustic properties and the proposed PnC sensor can detect such variations, thanks to Fano interference effect. To make the physical model less complex and emphasize more on employing Fano interference in the development of PnC biosensors, we assume plane strain boundary condition and all the studies are conducted on the 2-D representative model. We also presented all the results

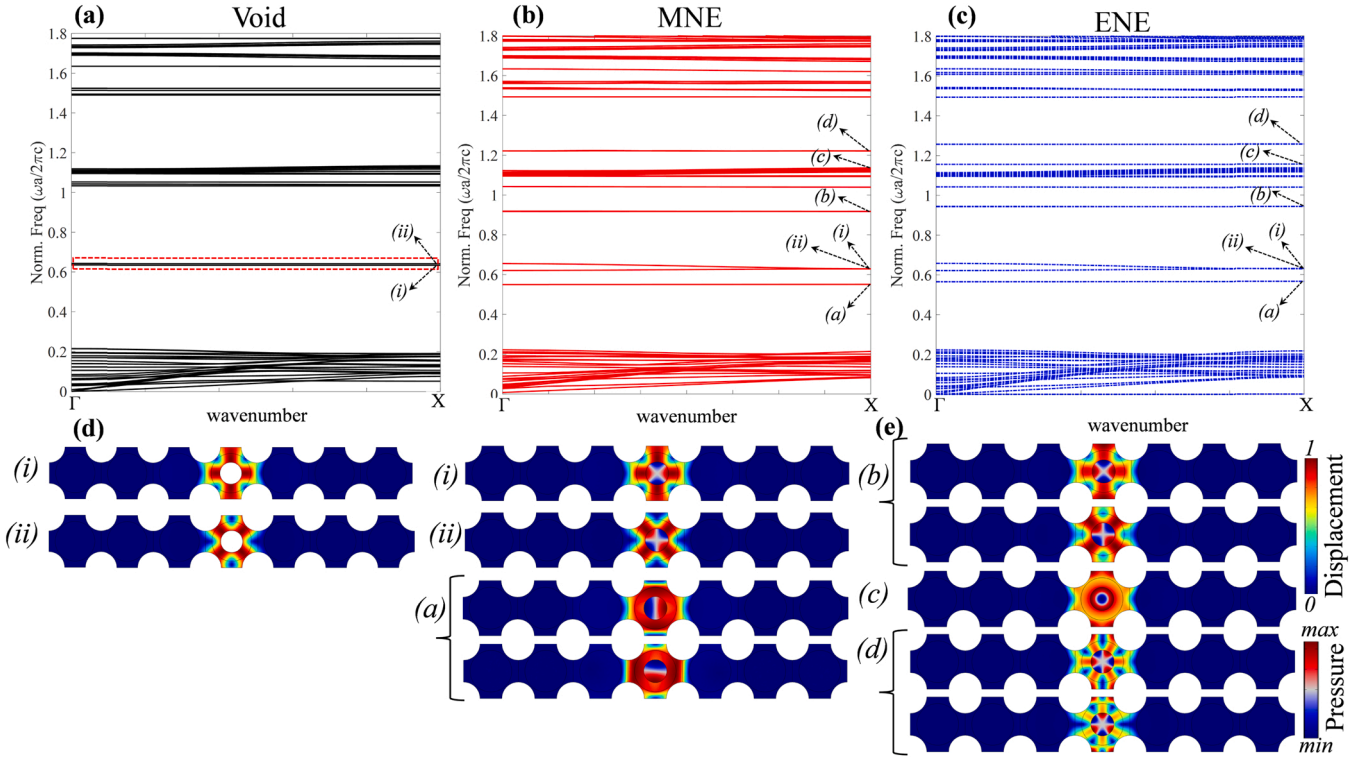

Fig. 5. Wave dispersion curve for supercell lattices with (a) localized cavity modes (*i*) and (*ii*) in solid. (b, c) The introduction of MNE and ENE inside the hollow tungsten inclusion results into three additional robust localize bands *a, b, c* positioned inside the first and second BGs. (d, e) Displacement (solid part) and pressure (liquid part) field distribution plots corresponding to the localize bands.

Table 2
Acoustic properties of MNE with varying temperature (10–40 °C). The data is obtained from Pin¯eiro et al. [37].

Temperature (°C)	Density (kg/m^3)			Wave velocity (m/sec)		
	0.1 MPa	50 MPa	100 MPa	0.1 MPa	50 MPa	100 MPa
10	1554	1659.65	1725.06	650.5	888.2	1046.5
15	1540	1648	1716.25	634	871.3	1034.6
20	1527	1641.99	1710.34	617	864.1	1025.6
25	1515	1633.17	1703.01	600.2	852.4	1015.0
30	1501	1624.39	1695.73	584	841.3	1004.9
35	1488	1614.2	1688.3	568	832.5	994.2
40	1474	1606.97	1681.38	551.7	819.1	985.5

Table 3
Acoustic properties of ENE with varying temperature (10–40 °C). The data is obtained from Pin¯eiro et al. [37].

Temperature (°C)	Density (kg/m^3)			Wave velocity (m/sec)		
	0.1 MPa	50 MPa	100 MPa	0.1 MPa	50 MPa	100 MPa
10	1455	1554.97	1616.88	669.9	910.1	1070.5
15	1445	1547.2	1608.5	650.2	902.4	1062.2
20	1438	1539.25	1603.55	638.2	888.8	1051.4
25	1433	1531.40	1596.92	622.6	877.1	1041.1
30	1415	1523.59	1590.34	607.4	867.0	1032.4
35	1398	1516.2	1584.5	592.3	855.4	1021.7
40	1383	1508.08	1577.33	575.5	846.1	1014.2

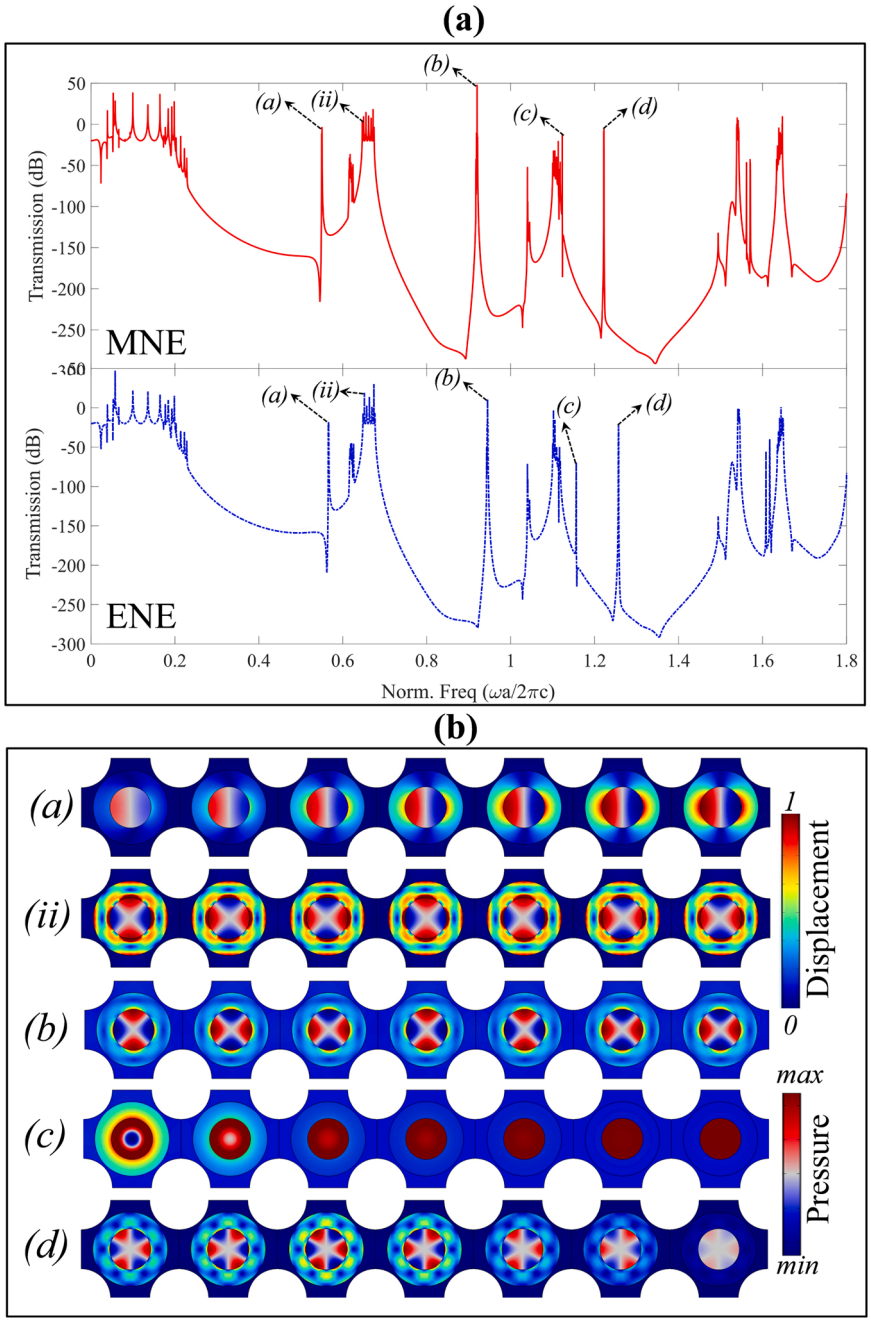

Fig. 6. Frequency response spectrum for supercell array where the void inside the Tungsten inclusion is filled with (a) MNE and ENE at temperature T = 10 °C and pressure 0.1 MPa. Fano interference asymmetrical transmission profile caused by wave interference can be seen for newly born localize modes. (b) Displacement and pressure distribution fields in solid and active solvents, respectively at the localize modes highlighted in the response spectra.

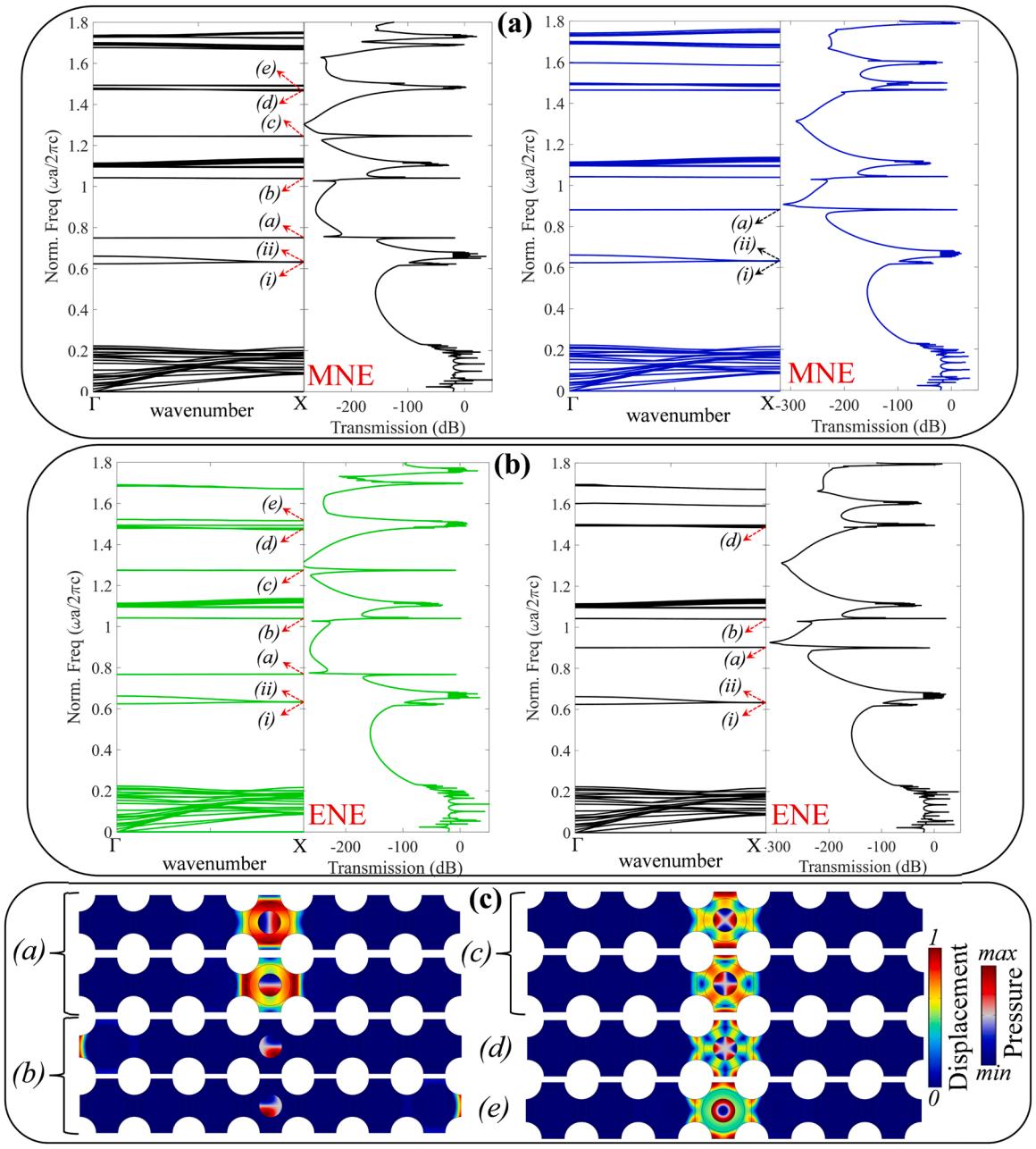

Fig. 7. Wave dispersion curves and transmission spectra for supercell lattice structure where the central unit cell structure is filled with MNE and ENE solvents. (a) MNE with (left) 50 MPa (right) 100 MPa. (b) ENE with (left) 50 MPa (right) 100 MPa. The temperature is kept as T $= 10^{o}C$. The Fano interference asymmetrical transmission profile for both solvents are highlighted in the transmission curve. (c) The corresponding displacement and pressure field plots are shown where wave energy localization can be observed.

in the form of normalized frequency $\omega a/2\pi c$ where $c = \sqrt{E/\rho}$ is wave velocity in Epoxy matrix. The future study tends to look into the development of 3-D numerical and experimental models for real-time performance investigation.

The remaining paper is organized as follows. Section 1 is introduction. The PnC unit cell structure and modeling approach is given in Section 2. Section 3 discusses the dispersion curve and cavity mode of the proposed PnC bio-chemical sensor. The incorporation of the MNE and ENE solvents inside the cavity for sensing application and Fano resonance phenomena are discussed in Section 4. Finally, the conclusion is given in Section 5.

2. Design and modeling strategy

Fig. 1(a-c) shows the composite PnC structure proposed. The unit cell structure consists of soft Epoxy matrix that contains heavy inclusion as Tungsten. Prior studies [30,34] show that such combination induce low frequency wide BGs. The material parameters are given in Table 1. The associated geometric parameters for unit cell structure is given at the inset of Fig. 1. The periodic array of hole with radius r_h is drilled inside the Epoxy plate. Although we consider the lattice constant $a = 1\ mm$, all the results are normalized for better understanding and application. To generate defect mode, a circular hole of radius r is made inside the Tungsten inclusion with filling ratio $f_o = \frac{\pi r^2}{a^2 - \pi r_h^2}$. According to previous works [30,35,36], such structural modification result into passband inside the BG region and give birth to localize cavity mode with strong

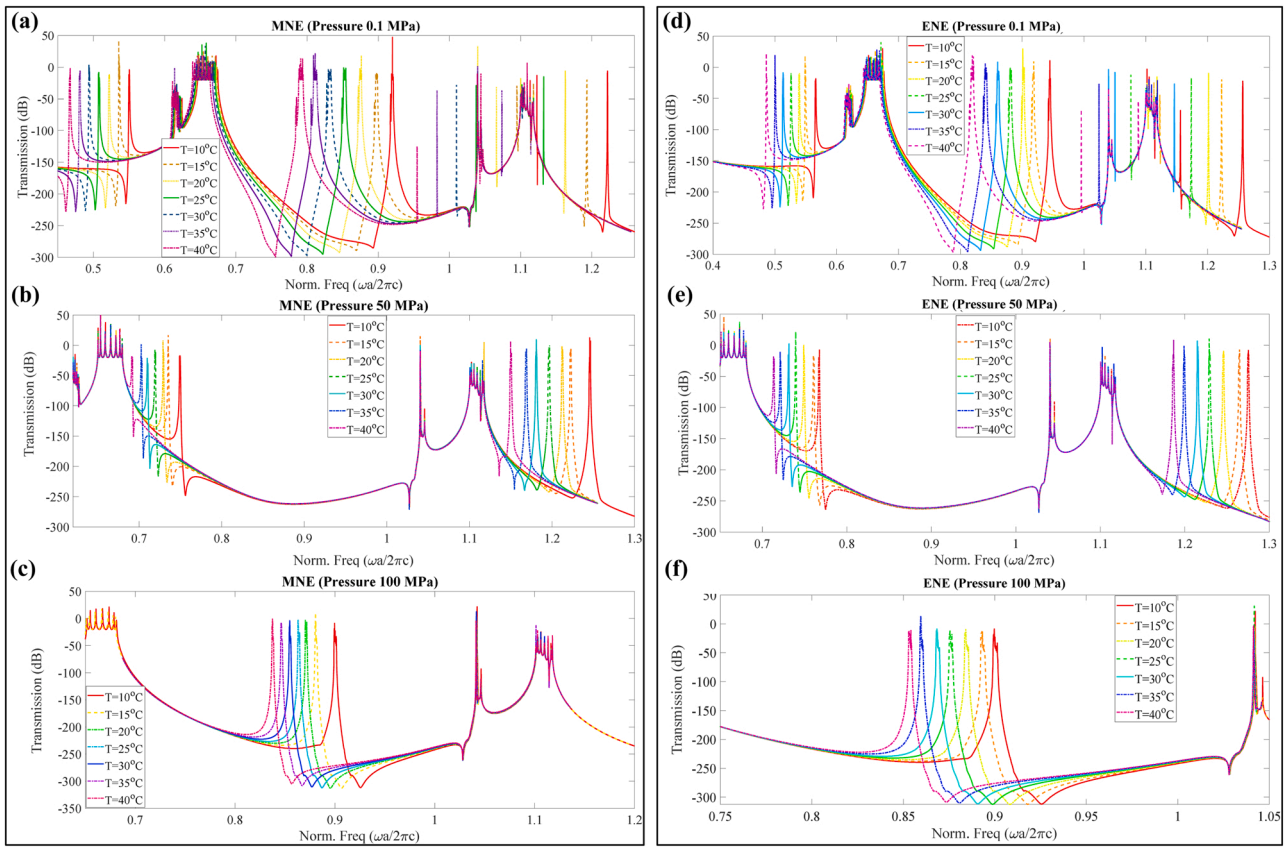

Fig. 8. Evolution of Fano like asymmetric transmission peaks with change in MNE and ENE temperature (10–40 °C) when pressure is kept (a, d) 0.1 MPa (b, e) 50 MPa (c, f) 100 MPa.

wave energy localization. To convert this cavity mode into PnC bio-chemical sensor, one can fill the hole with desirable solvents like MNE and ENE whose acoustic properties need to be detected, see Fig. 1 (c). Here, in this study we propose a methodology on how Fano interference can generate robust asymmetric peaks in the transmission profile upon coupling of incident wave with scattered wave field caused by the presence of active solvent. By using Fano interference mechanism, we capture the variation in acoustic property of MNE and ENE with change in temperature and pressure. The variation of acoustic properties subject to change in temperature and compressed MNE and ENE is calculated experimentally by Pin¯eiro et al. [37]. Our proposed PnC based bio-chemical sensor approach and research methodology can be applied to capture the changes in acoustic property of other solvents too. For better understanding of readership, array of unit cell structure with cavity and in-filled MNE/ENE is shown in Fig. 1(d).

Since numerous studies have reported theoretical model to solve the wave dispersion relation for the proposed unit cell structures, the detailed theoretical formulations are outside the scope of this work. Interested readers may refer to Hussein et al. [38]. This study is conducted by finite element based numerical simulation using commercially available code COMSOL Multiphysics. We used COMSOL fluid-structure interaction physics module that combines solid mechanics with pressure acoustic model to form a multiphysics coupling. For wave dispersion curve, eigenfrequency study is implemented where for each wave vector in the irreducible Brillouin zone [39], eigenfrequency is calculated. We applied Floquet-Bloch periodicity condition on the vertical edges of the unit cell structure, see Fig. 1(a-c). To obtain frequency response spectrum, frequency domain study setting is used on array of seven unit cell structures, see Fig. 1(e). The displacement fields at the input (beginning of array where harmonic excitation is applied) and output (last unit cell structure in the array) probe edges are recorded and wave transmission curve is plotted, see Fig. 1(e). The transmission spectrum is calculated as $20\log 10\left(\frac{u_{out}}{u_{in}}\right)$ where u_{out} and u_{in} are displacement at the output and input probes. We found COMSOL direct solver (PARDISO) quite useful and robust for this type of Multiphysics problems as compared to MUMPS solver. MUMPS is quite efficient for solid mechanics, acoustics and other single physics-based problems. Moreover, MUMPS is computationally quick compared to PARDISO for a small number of available CPUs. However, for larger number of CPUs, PARDISO is found more efficient than MUMPS. So, for vibracoustic problems one need to be careful with selection of direct solver types based on available computation resources. About mesh, we adopted COMSOL default triangular element with extra fine size.

3. Dispersion curve and cavity mode

Wave dispersion curve is a graphical representation of wavenumber with counterpart eigenmodes. For the square lattice arrangement of PnC considered, the dispersion curve for parent unit cell structure (see Fig. 1 (a)) is shown in Fig. 2. We have obtained two wide complete BGs with central frequencies around $\omega a/2\pi c = 0.6$ and $\omega a/2\pi c = 1.4$, respectively. The wave transmission curve is also shown aside the dispersion plot and one can observe drastic amount of wave attenuation inside the BG frequency regions. This validate the efficacy of the obtained BGs.

Next, we drilled a hole of radius r inside the Tungsten inclusion and studied the wave dispersion property. The wave dispersion plot showed birth of two new passbands inside the first BG as shown in Fig. 3. Furthermore, the wave transmission spectrum confirmed the presence of sharp wave transmission peaks corresponding to these newly born localized passbands. We named these newly born localized cavity modes as mode (*i*) and (*ii*) for easy understanding. The displacement field plot shows that at these localized modes, the wave energy is confined inside

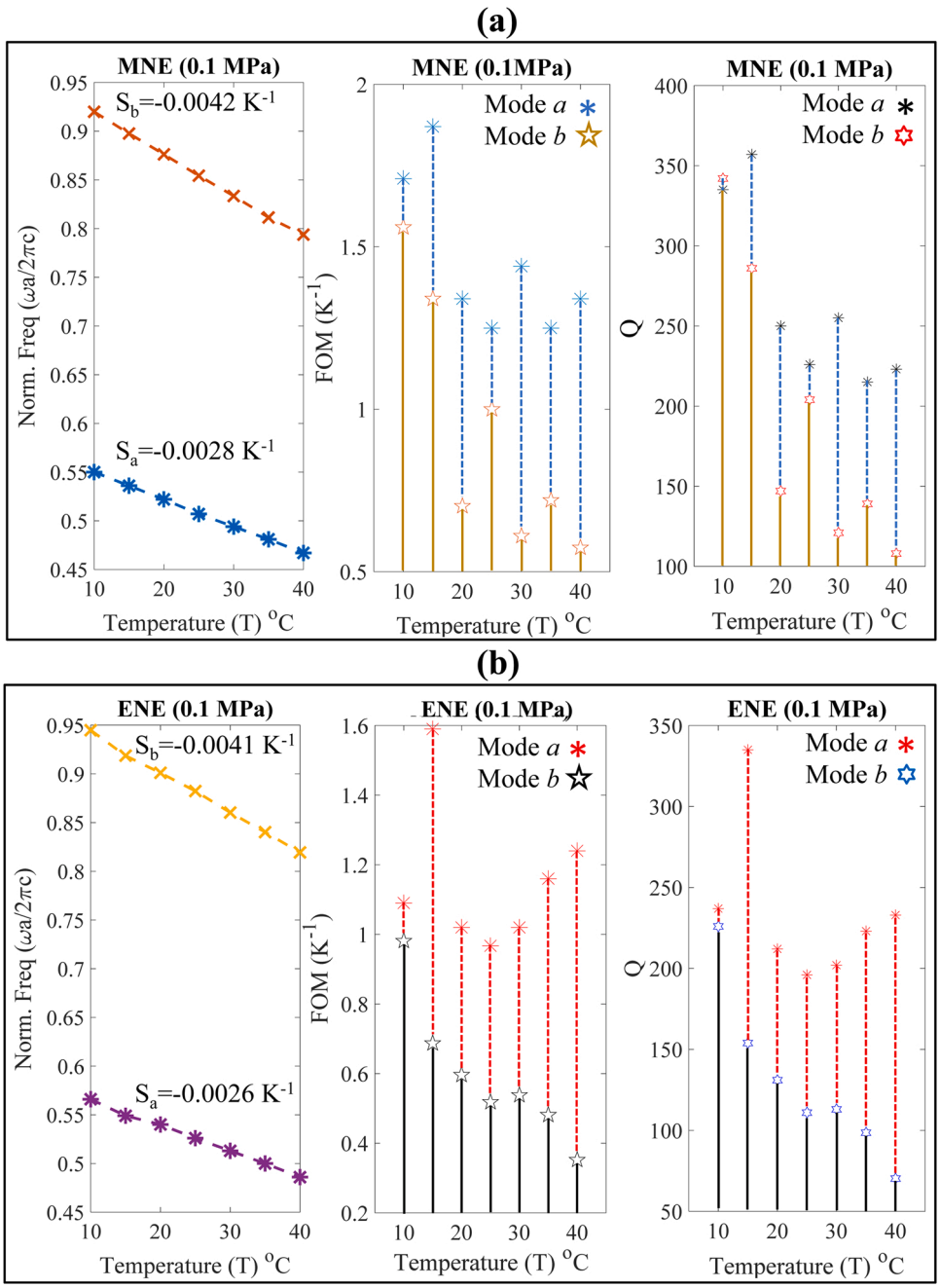

Fig. 9. Performance quantification of the proposed acoustic bio-chemical sensor subjected to (a) MNE and (b) ENE solvents. The evolution of Fano-interference mode (a) and (b) with varying temperature is shown. The sensitivities, FOM and Q-factor calculated are depicted at the inset of figure.

the cavity modes and no wave propagation is witnessed in the neighboring unit cell structures. This is due to the fact that, these localize modes lie inside the BG of parent unit cell structure. As reported by Jin et al. [35] for Lamb wave in pillar-plate model and later by Muhammad et al. [36] for surface waves, the mode (i) is also called deaf band because this is not excited by input excitation. Therefore, no transmission peak can be witnessed in the wave transmission profile.

The position of these localize bands are dependent on the hole of radius r drilled inside the Tungsten inclusion. An increase in r will shift the localize bands to lower frequency region. While smaller r will position these bands to higher frequency spectrum [35]. Like for $r = 0.1a$, the localize mode (i) and (ii) will be positioned inside the second BG, see Fig. 4. To keep these localized cavity modes in the center of first BG, we choose $r = 0.21a$ as highlighted by black dashed line in Fig. 4. Moreover, it is to be noted that these bands are solid cavity modes and has no relation with presence of active solvents like MNE and ENE whose acoustic properties is to be captured. In fact, when this cavity will be filled with some active solvents, again these bands will not disappear, see Fig. 5.

4. Solid-fluid interaction

In this section we will discuss about usefulness of cavity modes in sensing applications and link it with the birth of Fano interference that generate robust asymmetric transmission profile at low frequency region upon introduction of active solvents like MNE and ENE. First, we will give a general overview about PnC bio-chemical sensor design and working mechanism, mainly focusing on the concept of Fano interference. Then by using a case study on the MNE and ENE solvents, we will discuss the proof of this concept where these solvents are subjected to

varying pressure and temperature fields. Further, an analysis on sensitivity and figure of merit (FOM) is covered to show the potentiality of this approach for bio-chemical sensing applications.

4.1. Effect of fluid acoustic property on localize modes

The wave dispersion curves discussed in the prior section is based on the eigenfrequency study performed on a single infinitely periodic unit cell structure, see Fig. 1(a-c). We also construct a finite array of supercell structure that consists of seven unit cells where the hollow tungsten inclusion is placed at the center, see Fig. 1(d). The Floquet-Bloch periodicity condition is applied on the *y*-direction to make it infinitely periodic. Fig. 5(a) shows the dispersion curve for supercell lattice in the $\Gamma - X$ direction of the Brillouin zone. Similar to Fig. 3, one can observe presence of localized cavity bands (*i*) and (*ii*) inside the first BG. The displacement field plot for these bands are shown in Fig. 5(c) and these are reminiscent to results depicted in Fig. 3.

Next, we fill the hollow tungsten inclusion with some active solvent whose acoustic properties need to be detected. In this case, we stick to MNE and ENE solvents whose properties are obtained from experimental results reported by Pin¯eiro et al. [37]. The dispersion curve for supercell lattice (see Fig. 1(d)) is obtained and we observed presence of multiple newly born localized bands like band (*a-c*) inside first and second BGs apart from the solid cavity bands (*i*) and (*ii*). The origin of these modes can be understood by inspecting the eigenmodes at reported frequencies. The acoustic displacement field modulus of MNE/ENE solvents can be deduce from the expression $\widetilde{u} = \frac{1}{\widehat{\rho}_s \omega^2} \nabla \bar{p}$ where $\widetilde{u}$ is acoustic displacement field, $\widehat{\rho}_s$ is density of the solvent, ω is angular frequency and $\bar{p}$denotes acoustic pressure.

The displacement field plots show that mode (*i*) and (*ii*) is positioned at the identical frequency, see Fig. 3. However, the other localize bands are formed due to introduction of the MNE and ENE solvents. They are generated due to coupling of incident wave with scattered wave fields caused by presence of active solvent resulting into Fano interference effect. The displacement fields in solid and pressure in fluid are depicted with two different color bars. From displacement field plots shown in Fig. 5(d), one can observe the localization of wave energy around the MNE and ENE solvents and no wave propagation is witnessed in the neighboring unit cell structures. These newly born asymmetric bands have stronger wave energy localization as compared to solid-air cavity modes (*i*) and (*ii*) due to occurrence of Fano interference effect caused by interaction of incident and scattered wave fields. The position of these bands are dependent upon acoustic property of the MNE and ENE solvents. Any variation in acoustic properties will alter the position of these localize bands. Further details are given in the next section. For bio-chemical sensing applications, it is important that these localize bands must be present inside the BG frequency region. In order to achieve this goal, depending upon the property of active solvent, one should alter the physical and geometric parameters of the unit cell structure. This can be done by optimizing the unit cell structure to position the BG in the required frequency region.

4.2. Case study

Based on the findings reported in Section 4.1, here we consider two active solvents MNE and ENE to examine the performance of proposed PnC bio-chemical sensor. Since MNE and ENE are important solvents with wide range of applications in cosmetic, biochemicals and pharmaceutical products and the variation in acoustic property with temperature is known [37], see Tables 2 and 3, we applied the designed PnC bio-chemical sensor to capture the acoustic properties of these two solvents with change in temperature and pressure. Fig. 6 shows the frequency response spectrum for supercell lattice filled with MNE and ENE solvents where harmonic excitation is applied on the left end and response is recorded on the right end (output probe). For the shown transmission spectra, the temperature is $T = 10^oC$ and applied pressure is 0.1 MPa. The transmission spectrum depicts presence of asymmetrical transmission profile like mode (*a*) that is generated by Fano interference resulting from wave interference and this particular mode is positioned at relatively low frequency region. We also observed a sharp transmission peak for mode (*b*) in the second BG that is associated to quadrupole Fano interference [19]. Likewise, at relatively higher frequency region, other modes (*c*, *d*) is also observed that is associated to localize mode of the active solvents. It is to be noted that these modes are generate by Fano interference mechanism due to presence of MNE and ENE solvents inside the cavity. If these solvents from the cavity is removed, such robust asymmetrical transmission peaks will diminish. Therefore, presence of MNE/ENE is crucial for the birth of Fano interference effect, that makes this approach promising for sensing application.

For MNE and ENE solvents Pin¯eiro et al. [37] performed experimental tests to study the effect of temperature and pressure on acoustic properties. The wave dispersion curve and transmission spectra depicted in Fig. 6 is corresponding to temperature $T = 10^oC$ and pressure of compressed solvent remains 0.1 MPa. Here we kept the temperature constant i.e., $T = 10^oC$ and change the pressure of active solvent for both MNE and ENE to 50 MPa and 100 MPa in order to observe the variation on wave transmission profile. Fig. 7(a-b) shows the dispersion curve and wave transmission spectra for supercell lattice. The lattice consists of seven-unit cell structure where the Tungsten inclusion filled with MNE/ENE is placed at the center, see Fig. 1(d). Reminiscent to Fig. 6, when pressure is kept 50 MPa for both MNE and ENE solvents, we observed asymmetric transmission profiles inside the first and second BGs. Except solid modes (*i*) and (*ii*), the position of these localize bands have changed. It shows that an increase in pressure shift the localize bands induced by presence of MNE/ENE to higher frequency region.

Furthermore, when pressure is set to 100 MPa, the Fano interference mode (*a*) move to relatively higher frequency region as compared to prior case. In general, for both MNE and ENE, it is observed that an increase in pressure shift the localize bands to higher frequency region. The displacement and pressure field plots corresponding to these newly born localize modes are shown in Fig. 7(c). The robust localization of acoustic wave energy at the central unit cell structure bounded by MNE and ENE solvents is observed.

4.3. Effect of temperature and pressure on Fano interference asymmetrical profile

Next, we investigate the effect of temperature on the wave transmission profile and try to detect the variation in acoustic properties. Again, the experimental results by Pin¯eiro et al. [37] is used and we consider seven temperature values as $T = 10, 15, 20, 25, 30, 35, 40^oC$. The effect of temperature is plotted for three different values of applied pressure 0.1 MPa, 50 MPa, 100 MPa as shown in Fig. 8(a-f). This also manifest the findings discussed in the prior section. It is found that with increase in temperature, the solvent based localize modes shift to lower frequency region. This follows Helmholtz resonator type behavior where the resonance frequency is directly proportional to speed of acoustic wave and inversely proportional to the volume [40]. As shown in Tables 2 and 3, acoustic wave velocity reduces with increase in temperature. Therefore, the Fano-interference frequency shifts to lower frequency region for higher temperature values. The shift in frequency comes from velocity of the MNE and ENE solvents instead of the mass density. Likewise, if one reduces the cavity size where MNE and ENE solvents are filled, this will move the Fano-interference to higher frequency region. Similar findings are reported by Amoudache et al. [21] for 1-Methyl-3-octylimidazolium Chloride in Methanol for different molar ratio. This shift in frequency is observed for the acoustic Fano-like interference modes mainly localized in the infilled solvents. The mode with acoustic field localization caused by solid-air cavity i.e., modes (*i*) and (*ii*) remain unchanged. It is also observed that an increase in

pressure shift the Fano-like interference profile to higher frequency region due to increase in wave velocity, see Tables 2 and 3.

4.4. Sensor performance

Fig. 9 shows the evolution of Fano-interference modes (*a*) and (*b*) with temperature for MNE and ENE solvents at 0.1 MPa. A linear behavior with negative slope is observed that indicate, increase in temperature of solvent shifts the Fano-interference modes (*a*) and (*b*) to lower frequency region. From this graph the sensitivity $S = \Delta f/\Delta T$ can be quantified as shown at the inset of Fig. 9. The sensitivity of the sensor alone is not enough to fully characterize the sensor performance. Instead, figure of merit $FOM = S.Q/f_r$ needs to be calculated where $Q = f_r/f_{1/2}$ is quality factor, f_r is frequency of Fano-interference profile and $f_{1/2}$ is frequency width. The FOM calculated in the presence of both solvents is shown in Fig. 9 and one can observe that mode (*a*) has comparatively better performance than mode (*b*). This shows the robustness of Fano-interference at low-frequency region. Further, the Fano interference effect at higher frequency region gives lower FOM and Q values. This also depends upon the temperature of MNE/ENE solvents, see Fig. 9. We assume identical findings can be obtained for other cases with different temperature and pressure fields. Fig. 9 validates the effectiveness of proposed acoustic bio-chemical sensor for bio-chemical sensing applications at low frequency region.

5. Conclusion

A conceptual framework for new type of acoustic bio-chemical sensor to detect the variations in acoustic properties of active solvents like MNE and ENE is studied by applying the concept of phononic crystals and metamaterials. The Fano-like interference effect that resulted into asymmetrical transmission profile is observed at relatively low frequency region when MNE and ENE solvents are introduced into the phononic crystal composite structure. The asymmetrical transmission peak is observed due to coupling of incident wave and scatter wave emitted from the solid fluid coupling of active solvents. The variation in room temperature and pressure affect the acoustic properties of some solvents like MNE and ENE. The proposed phononic crystal based acoustic bio-chemical smart sensor can efficiently detect such variations, thanks to bandgap property of phononic crystal and metamaterials. It is found that with increase in temperature, the wave speed of MNE and ENE decreases that eventually shift the Fano-interference profile to low-frequency region. In contrast, an increase in pressure has opposite effect due to wave speed. The shift in Fano-interference frequency is influenced by wave speed in MNE and ENE rather than density of active solvents. The proposed sensor sensitivity, figure of merit and quality factor is also determined that further corroborate our findings. Although the conceptual framework of acoustic bio-chemical sensor is applied to MNE and ENE solvents, proposed research methodology can be applied to detect variation in acoustic properties of some other active fluids. Such strategy can be useful in pharmaceutical production, petrochemicals, capturing ingredients of cosmetic and beauty products etc. and other bio-chemical applications. The future works will focus on replication of these findings to 3-D physical model and development of experiment setup to validate this concept for bio-chemical acoustic sensor development.

CRediT authorship contribution statement

Muhammad: Conceptualization, Data curation, Formal analysis, Funding acquisition, Investigation, Methodology, Project administration, Resources, Software, Supervision, Validation, Visualization, Writing – original draft, Writing – review & editing.

Declaration of Competing Interest

The authors declare that they have no known competing financial interests or personal relationships that could have appeared to influence the work reported in this paper.

Data availability

Data will be made available on request. The data that supports the findings of this study are available from the corresponding author upon reasonable request.

Acknowledgements

The work described in this paper was supported by Irish Research Council-Enterprise Partneship Scheme Postdoctoral Fellowship Scheme, Republic of Ireland (Project No. 211705 Award 16976).

References

[1] M.S. Kushwaha, P. Halevi, G. Martinez, L. Dobrzynski, B. Djafari-Rouhani, Theory of acoustic band structure of periodic elastic composites, Phys. Rev. B Condens. Matter 49 (4) (1994) 2313–2322.
[2] Z. Liu, X. Zhang, Y. Mao, Y.Y. Zhu, Z. Yang, C.T. Chan, P. Sheng, Locally resonant sonic materials, Science 289 (5485) (2000) 1734–1736.
[3] Muhammad, C.W. Lim, From photonic crystals to seismic metamaterials: a review via phononic crystals and acoustic metamaterials, Arch. Comput. Methods Eng. 29 (2022) 1137–1198.
[4] J. Yabin, P. Yan, B. Bernard, H. Hossein, D. Leonard, D.-R. Bahram, I.H. Mahmoud, Physics of surface vibrational resonances: pillared phononic crystals, metamaterials, and metasurfaces, Rep. Prog. Phys. (2021).
[5] A.H. Aly, A. Nagaty, A. Mehaney, One-dimensional phononic crystals that incorporate a defective piezoelectric/piezomagnetic as a new sensor, Eur. Phys. J. B 91 (10) (2018) 211.
[6] A. Nagaty, A. Mehaney, A.H. Aly, Influence of temperature on the properties of one-dimensional piezoelectric phononic crystals, Chin. Phys. B 27 (9) (2018), 094301.
[7] A.H. Aly, A. Nagaty, Z. Khalifa, A. Mehaney, The significance of temperature dependence on the piezoelectric energy harvesting by using a phononic crystal, J. Appl. Phys. 123 (18) (2018), 185102.
[8] Y.Q. Fu, J.K. Luo, N.T. Nguyen, A.J. Walton, A.J. Flewitt, X.T. Zu, Y. Li, G. McHale, A. Matthews, E. Iborra, H. Du, W.I. Milne, Advances in piezoelectric thin films for acoustic biosensors, acoustofluidics and lab-on-chip applications, Prog. Mater. Sci. 89 (2017) 31–91.
[9] Q. Lin, F. Cai, F. Li, D. Zhao, X. Xia, W. Zhou, L. Meng, H. Zheng, The compact acoustic liquid sensor based on the circumferential modes of a cylindrical shell, Sens. Actuators A Phys. 304 (2020), 111843.
[10] H. Gharibi, A. Khaligh, A. Bahrami, H.B. Ghavifekr, A very high sensitive interferometric phononic crystal liquid sensor, J. Mol. Liq. 296 (2019), 111878.
[11] H. Gharibi, A. Mehaney, Two-dimensional phononic crystal sensor for volumetric detection of hydrogen peroxide (H2O2) in liquids, Phys. E Low Dimens. Syst. Nanostruct. 126 (2021), 114429.
[12] H. Gharibi, A. Mehaney, A. Bahrami, High performance design for detecting NaI–water concentrations using a two-dimensional phononic crystal biosensor, J. Phys. D Appl. Phys. 54 (1) (2020), 015304.
[13] A. Oseev, M. Zubtsov, R. Lucklum, Gasoline properties determination with phononic crystal cavity sensor, Sens. Actuators B Chem. 189 (2013) 208–212.
[14] Y. Jin, Y. Pennec, Y. Pan, B. Djafari-Rouhani, Phononic crystal plate with hollow pillars actively controlled by fluid filling, Crystals 6 (2016) 6.
[15] N. Mukhin, M. Kutia, A. Oseev, U. Steinmann, S. Palis, R. Lucklum, Narrow band solid-liquid composite arrangements: alternative solutions for phononic crystal-based liquid sensors, Sensors 19 (17) (2019) 3743.
[16] U. Fano, Effects of configuration interaction on intensities and phase shifts, Phys. Rev. 124 (6) (1961) 1866–1878.
[17] M.F. Limonov, Fano resonance for applications, Adv. Opt. Photon. 13 (3) (2021) 703–771.
[18] M.F. Limonov, M.V. Rybin, A.N. Poddubny, Y.S. Kivshar, Fano resonances in photonics, Nat. Photonics 11 (9) (2017) 543–554.
[19] B. Luk'yanchuk, N.I. Zheludev, S.A. Maier, N.J. Halas, P. Nordlander, H. Giessen, C.T. Chong, The Fano resonance in plasmonic nanostructures and metamaterials, Nat. Mater. 9 (9) (2010) 707–715.
[20] A.H. Aly, D. Mohamed, H.A. Elsayed, A. Mehaney, Fano resonance by means of the one-dimensional superconductor photonic crystals, J. Supercond. Nov. Magn. 31 (12) (2018) 3827–3833.
[21] S. Amoudache, R. Moiseyenko, Y. Pennec, B.D. Rouhani, A. Khater, R. Lucklum, R. Tigrine, Optical and acoustic sensing using Fano-like resonances in dual phononic and photonic crystal plate, J. Appl. Phys. 119 (11) (2016), 114502.
[22] Y. Jin, E.I.H. Ei Boudouti, Y. Pennec, B. Djafari-Rouhani, Tunable Fano resonances of Lamb modes in a pillared metasurface, J. Phys. D Appl. Phys. 50 (42) (2017), 425304.

[23] M. Oudich, B. Djafari-Rouhani, B. Bonello, Y. Pennec, S. Hemaidia, F. Sarry, D. Beyssen, Rayleigh waves in phononic crystal made of multilayered pillars: confined modes, fano resonances, and acoustically induced transparency, Phys. Rev. Appl. 9 (3) (2018), 034013.
[24] S.E. Zaki, A. Mehaney, H.M. Hassanein, A.H. Aly, Fano resonance based defected 1D phononic crystal for highly sensitive gas sensing applications, Sci. Rep. 10 (1) (2020) 17979.
[25] A.E. Miroshnichenko, S. Flach, Y.S. Kivshar, Fano resonances in nanoscale structures, Rev. Mod. Phys. 82 (3) (2010) 2257–2298.
[26] K. Lodewijks, J. Ryken, W. Van Roy, G. Borghs, L. Lagae, P. Van Dorpe, Tuning the Fano resonance between localized and propagating surface plasmon resonances for refractive index sensing applications, Plasmonics 8 (3) (2013) 1379–1385.
[27] Z.L. Sámson, K.F. MacDonald, F.D. Angelis, B. Gholipour, K. Knight, C.C. Huang, E. D. Fabrizio, D.W. Hewak, N.I. Zheludev, Metamaterial electro-optic switch of nanoscale thickness, Appl. Phys. Lett. 96 (14) (2010), 143105.
[28] M. Oudich, B. Djafari-Rouhani, B. Bonello, Y. Pennec, F. Sarry, Phononic crystal made of multilayered ridges on a substrate for rayleigh waves manipulation, Crystals 7 (12) (2017) 372.
[29] C. Goffaux, J. Sánchez-Dehesa, A.L. Yeyati, P. Lambin, A. Khelif, J.O. Vasseur, B. Djafari-Rouhani, Evidence of Fano-like interference phenomena in locally resonant materials, Phys. Rev. Lett. 88 (22) (2002), 225502.
[30] Muhammad, C.W. Lim, A.Y.T. Leung, Plane and surface acoustic waves manipulation by three-dimensional composite phononic pillars with 3D bandgap and defect analysis, Acoustics 3 (1) (2021) 25–41.
[31] M. Ke, M. Zubtsov, R. Lucklum, Sub-wavelength phononic crystal liquid sensor, J. Appl. Phys. 110 (2) (2011), 026101.
[32] J. Arai, A novel non-flammable electrolyte containing methyl nonafluorobutyl ether for lithium secondary batteries, J. Appl. Electrochem. 32 (10) (2002) 1071–1079.
[33] S. Fang, G. Wang, L. Qu, D. Luo, L. Yang, S.-i Hirano, A novel mixture of diethylene glycol diethylether and non-flammable methyl-nonafluorobutyl ether as a safe electrolyte for lithium ion batteries, J. Mater. Chem. A 3 (42) (2015) 21159–21166.
[34] Muhammad, C.W. Lim, Dissipative multiresonant pillared and trampoline metamaterials with amplified local resonance bandgaps and broadband vibration attenuation, J. Vib. Acoust. 142 (6) (2020), 061012.
[35] Y. Jin, N. Fernez, Y. Pennec, B. Bonello, R.P. Moiseyenko, S. Hémon, Y. Pan, B. Djafari-Rouhani, Tunable waveguide and cavity in a phononic crystal plate by controlling whispering-gallery modes in hollow pillars, Phys. Rev. B 93 (5) (2016), 054109.
[36] Muhammad, C.W. Lim, J.N. Reddy, E. Carrera, X. Xu, Z. Zhou, Surface elastic waves whispering gallery modes based subwavelength tunable waveguide and cavity modes of the phononic crystals, Mech. Adv. Mater. Struct. 27(13) 1053–1064.
[37] M.M. Piñeiro, F. Plantier, D. Bessières, J.L. Legido, J.L. Daridon, High-pressure speed of sound measurements in methyl nonafluorobutyl ether and ethyl nonafluorobutyl ether, Fluid Phase Equilibria 222–223 (2004) 297–302.
[38] M.I. Hussein, M.J. Leamy, M. Ruzzene, Dynamics of phononic materials and structures: historical origins, recent progress, and future outlook, Appl. Mech. Rev. 66 (4) (2014), 040802.
[39] Muhammad, C.W. Lim, J.N. Reddy, Built-up structural steel sections as seismic metamaterials for surface wave attenuation with low frequency wide bandgap in layered soil medium, Eng. Struct. 188 (2019) 440–451.
[40] T. Persoons, General reduced-order model to design and operate synthetic jet actuators, Aiaa J. 50 (4) (2012) 916–927.